Charging Mechanisms of Trapped Element-Selectively Excited Nanoparticles Exposed to Soft X Rays

M. Grimm,[1,2,*] B. Langer,[1,2] S. Schlemmer,[3] T. Lischke,[4] U. Becker,[4] W. Widdra,[5] D. Gerlich,[6] R. Flesch,[1] and E. Rühl[1]

[1]*Institut für Physikalische Chemie, Universität Würzburg, Am Hubland, 97074 Würzburg, Germany*

[2]*Max-Born-Institut für Nichtlineare Optik und Kurzzeitspektroskopie, Max-Born-Strasse 2a, 12489 Berlin, Germany*

[3]*Fakultät für Physik, Universität zu Köln, Zülpicher Strasse 77, 50937 Köln, Germany*

[4]*Fritz-Haber-Institut der Max-Planck-Gesellschaft, Faradayweg 4-6, 14195 Berlin, Germany*

[5]*Fachbereich Physik, Martin-Luther-Universität Halle-Wittenberg, 06099 Halle, Germany*

[6]*Institut für Physik, Technische Universität Chemnitz, Reichenhainer Str. 70, 09107 Chemnitz, Germany*

(Received 11 August 2005; published 13 February 2006)

Charging mechanisms of trapped, element-selectively excited free SiO_2 nanoparticles by soft x rays are reported. The absolute charge state of the particles is measured and the electron emission probability is derived. Changes in electron emission processes as a function of photon energy and particle charge are obtained from the charging current. This allows us to distinguish contributions from primary photoelectrons, Auger electrons, and secondary electrons. Processes leading to no change in charge state after absorption of x-ray photons are identified. O 1*s*-excited SiO_2 particles of low charge state indicate that the charging current follows the inner-shell absorption. In contrast, highly charged SiO_2 nanoparticles are efficiently charged by resonant Auger processes, whereas direct photoemission and normal Auger processes do not contribute to changes in particle charge. These results are discussed in terms of an electrostatic model.

DOI: 10.1103/PhysRevLett.96.066801 PACS numbers: 73.22.−f, 78.70.Dm

Nanoparticles cover the size regime between clusters and macroscopic condensed matter. Their unique electronic, structural, and chemical properties have been the subject of numerous recent works, where the particles are studied either in solution or they are deposited on substrates [1]. Recent work also includes investigations by soft x-ray spectroscopies, where structural disorder was studied [2]. It is well-known that intense, short wavelength radiation, such as high brilliance synchrotron radiation, leads to radiation induced damage as well as charging of the deposited nanoparticle samples, which may significantly change their properties [3]. This is especially true for small nanoparticles and quantum dots. Charging and photoionization of nanoparticles involving outer electronic shells has been investigated in the past by experimental and theoretical approaches [4–6]. Charging of free nanoparticles by x rays has been studied recently in an electrostatic precipitator [7]. This work indicates that direct photoelectric charging is relatively weak in a dense gas phase, whereas the attachment of ions to particles, corresponding to diffusion charging, dominates. Properties of isolated nano- and microparticles without any contact to a substrate are suitably investigated in traps [8–10]. This is of crucial importance for those properties, where contributions of the substrate dominate. Trap experiments also allow controlled charging using either electrons or ionizing radiation. In the case of insulators, charging may lead to substantial changes in electronic properties of matter [11].

We report in this Letter results on trapped nanoparticles, which allow us to vary their charge state in a controlled way, by using tunable soft x rays. First experiments on trapped, element-selectively excited nanoparticles are presented, where distinct changes in charge state are a result of direct photoelectric charging including the emission of secondary electrons. These results are used to derive charging mechanisms of free nanoparticles induced by soft x rays.

The experimental setup consists of a three-dimensional electrodynamic trap, which serves for nanoparticle storage in an ultrahigh vacuum setup, with a base pressure $<10^{-8}$ mbar during the experiments. The trap consists of two conical cap electrodes and eight rods, which replace the ring electrode of a classical three electrode Paul trap [8,12]. The ac voltage of the driving field is applied to the cone electrodes. A small loudspeaker below the trap serves as a particle reservoir as well as a particle injector. It is filled with monodisperse SiO_2 particles (Merck) of 498 ± 36 nm diameter [9]. The trapped particles typically carry initially some ten positive charges. They are illuminated by a frequency doubled Nd:YAG-laser ($P < 50$ mW, $\lambda = 532$ nm). The scattered light from the trapped particle is detected by an avalanche photodiode modulated by the secular motion frequencies ω_r and ω_z perpendicular and parallel to the trap axis, respectively. Both frequencies are obtained from a fast Fourier transform of the photodiode signal. At low photon flux the particle charge increases by one or integer multiples of the elementary charge (cf. Fig. 1). This allows us to determine both the absolute charge and the charge-to-mass ratio, and therefore the mass of the stored particle, where further details of this analysis are outlined in Refs. [8,13]. Upon mass and charge state characterization the particles are exposed to monochromatic synchrotron radiation in the soft x-ray regime (30–580 eV), using the U125/1-SGM- and UE52-SGM-beam lines at the storage ring BESSY-II (Berlin, Germany).

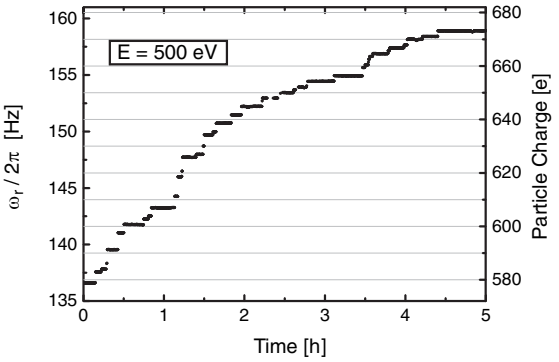

FIG. 1. Charge state of a trapped SiO_2 nanoparticle of 500 nm diameter upon x-ray illumination (500 eV) as determined by its secular motion frequency ω_r within an electrodynamic trap.

Figure 1 shows a typical charging curve of a single, trapped nanoparticle recorded at 500 eV photon energy. The charging curve shows distinct steps corresponding to changes in particle charge in multiples of the elementary charge e. We safely assume that under these conditions, i.e., at low photon flux, just single 500 eV-photons hit the particle. Note that this situation is different, if the photon flux is increased. The absence of downward steps in Fig. 1 indicates that at low charge state no charges are lost, e.g., by collisions with the residual gas or ion desorption.

Charging curves have been recorded at various photon energies ranging between 30 and 560 eV. Figures 2(a)–2(h) show a comparison of the step height distributions obtained from charging curves similar to that shown in Fig. 1. The charges on the particles are in each case <800, corresponding to a small surface potential of 0.25–4.9 V. The statistical analysis of the step heights yields the electron emission probability per absorbed photon. Note that the total 4π solid angle integrated emission probability is determined. The results indicate that the average step height per absorbed photon increases as a function of photon energy. This is straightforward since single ionization is expected to dominate at low photon energy, whereas double and multiple ionization occurs at increased photon energies, especially above the Si $2p$ edge ($E > 105$ eV). Figures 2(a)–2(c) have been recorded in the inner-valence regime, i.e., below the Si $2p$ edge. There, one observes a finite probability for the emission of two or more electrons per absorbed photon. This process is most likely due to the electron emission from different sites of the nanoparticle, where either secondary ionization of neighboring sites to the absorbing center by the photoelectron [14] or fast charge transfer processes may occur [15]. Direct double ionization involving the emission of two correlated electrons is expected to be of weak cross section, similar to photoionization of atoms (cf. Ref. [16]). Above the Si $2p$ edge LMM-Auger processes become active, whereas in the O $1s$ continuum KLL-Auger processes dominate. These processes lead efficiently to double and multiple ionization and the probability for the emission of secondary electrons

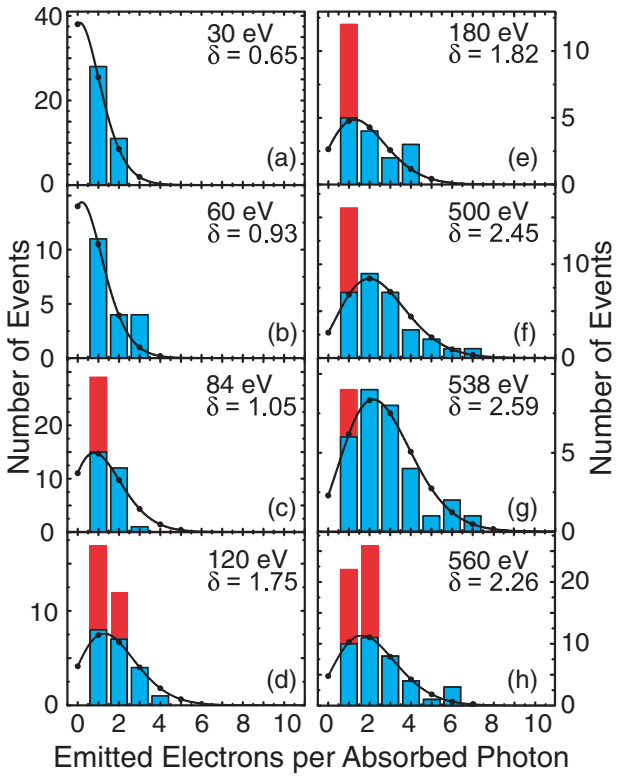

FIG. 2 (color). Step height distributions from charging curves at different photon energies. The height of the bars is obtained from the experimental results (cf. Fig. 1). The solid lines correspond to Poisson distributions, corresponding to the emission of secondary electrons. Contributions from direct photoionization and Auger processes are indicated in red. The average number of charging events per absorbed photon δ is indicated. See text for further details.

is also increased. As a result, the step heights increase with photon energy, so that up to 7 charges per absorbed photon are observed (cf. Fig. 2(g)], where the intensity of the multiple ionization events increases with photon energy.

The distributions of emitted secondary electrons per charging event are modeled by Poisson distributions, as indicated by full lines in Fig. 2. It is well-known that this is a suitable approach for the description of the electron emission statistics [17]. Poisson distributions are fitted to the experimental data by using $\Delta Q > +2$ events at $E > 60$ eV, since the primary photoelectrons and Auger electrons may affect the $\Delta Q \leq +2$ events, if they are emitted directly into the vacuum from near-surface sites. The Poisson distributions also show that there is a substantial probability of finding no change in charge state after photoabsorption. These events cannot be detected by the present experiment. Photoabsorption of soft x rays without any change in particle charge appears to be quite possible, since inelastically scattered electrons may either get thermalized in the bulk of the particles or in the case of highly charged ones the secondary electrons may get trapped due to Coulomb attraction. The Poisson distributions appear to

represent reasonable fits to the step height distributions for some photon energies. However, Figs. 2(c)–2(f) and 2(h) indicate that $\Delta Q = +1$ events are not suitably modeled by Poisson distributions. Further, the $\Delta Q = +2$ processes at 560 eV are also not well represented by the emission of secondary electrons. Intensity exceeding these distributions is marked by red color, reaching up to 40% of all emitted electrons. These processes are assigned to the emission of photoelectrons ($\Delta Q = +1$) and Auger electrons ($\Delta Q = +2$) [cf. Figs. 2(d) and 2(h)]. In contrast, slow photoelectrons do not contribute efficiently to charging. They are either formed at low photon energies in the inner-valence excitation regime ($\leq$60 eV) [cf. Figures 2(a) and 2(b)] and near core ionization energies, i.e., near the O 1s edge (cf. Figure 2(g)]. Thus, we can easily distinguish from charging curves the ionization processes contributing to changes in particle charge, i.e., direct photoionization and relaxation from the emission of secondary electrons. In all cases charging is predominantly due to the emission of secondary electrons, since these processes are expected to be dominant for bulk sites, where inelastic scattering dominates. The emission of primary electrons, i.e., photoelectrons and Auger electrons, can only come from near-surface sites.

The average number of emitted charges per charging events δ is determined from Fig. 2. The $\Delta Q = 0$ events are considered, as well. These are derived from the Poisson distributions. A characteristic photon energy dependence of δ is observed, ranging between 0.65 ± 0.3 and 2.59 ± 0.5, where the error limits are given by the limited number of charging events. The determined maximum of $\delta \sim 2.6$ and its position at 538 eV agrees well with the reference value [18].

Figure 3(a) shows the photon energy dependence of three representative charging curves, where three experiments with different initial and final charge states are reported (curves A–C). After setting the initial charge state, the photon energy was increased in constant time steps, while measuring the charge state. Note that the photon flux and the particle charge are considerably higher compared to the results displayed in Fig. 1. As a result, no steplike structures can be resolved because numerous electrons are emitted during the sample time of the fast Fourier transform. All curves A–C shown in Fig. 3(a) indicate that the slope of the charge state changes significantly at the O 1s edge, which is due to O 1s absorption [19–22]. The first derivative of the charging curves is shown in Fig. 3(b). These spectra are normalized to the photon flux. Furthermore, we have considered that the residual gas leads to a steady discharge of the particles at high charge states ($Q >$ 40 000); i.e., in this regime there is only a net charging current. At the lowest particle charge [curve A in Fig. 3(b)] we observe the characteristic near-edge features of SiO_2 absorption [19–22]. The maximum of the major asymmetric feature is located at 538.6 eV. This energy is in agreement with previous work, where various molecular final states contribute to this strong absorption band [20]. Moreover, there is a broad continuum resonance with a double hump structure peaking near 557 eV and 564.5 eV, which has also been found in previous work [22].

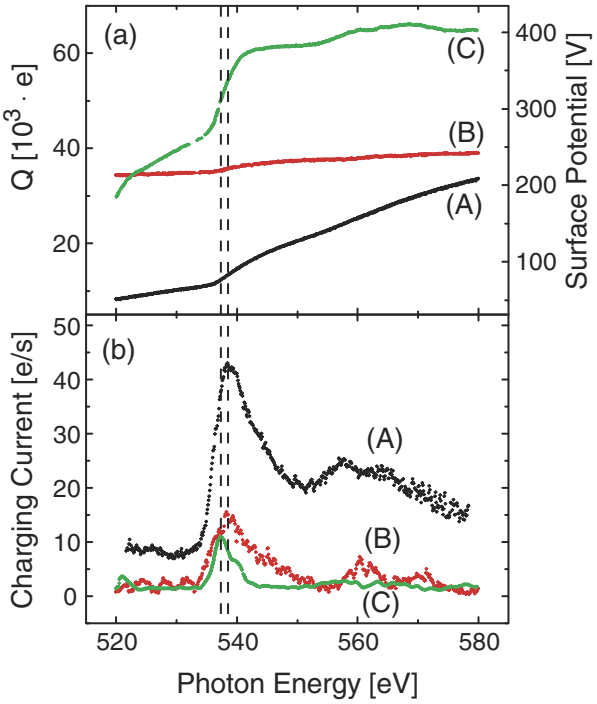

FIG. 3 (color online). (a) Charging curves as a function of photon energy of a differently charged SiO_2 nanoparticle. The curves A–C correspond to different initial and final charge states; (b) First derivative of the results shown in (a), corresponding to the charging current as a function of photon energy in the O 1s excitation regime. The left and right vertical dashed lines indicate the position of the maximum in curves (C) and (A), respectively.

Figure 3(b) (curve B) shows that the intensity of the charging current has substantially decreased compared to curve A, but the shape of the near-edge feature is still similar to that of curve A. The intensity in the O 1s continuum is decreased and the continuum resonances are barely visible. This indicates that considerably less charges are emitted from a particle that carries ~35 000 charges. Evidently, the surface potential, which is estimated to be 250 V assuming that the charges remain on the surface of the spherical particle, retains $85\% \pm 5\%$ of the emitted charges. This value is estimated from the changes in charging current shown in Fig. 3(b). Mostly low energy electrons, which originate from inelastically scattered photoelectrons and Si LMM-Auger electrons, are retained by the electric field of the charged particles. All other electrons are expected to have sufficient kinetic energy to be emitted above the vacuum level and contribute to the charging current and to an increase of the particle charge. Similarly, curve C shows that there is a further decrease in charging current, if the initial particle charge is increased

to about 50 000 charges at 538 eV photon energy. As a result, only ~5% of the electron charging current is observed in the O 1*s* regime compared to curve A. There is hardly any charging current in the O 1*s* continuum and the maximum of the intense resonance is redshifted by ~1 eV relative to that shown in spectrum A (cf. vertical dashed lines in Fig. 3). Note that the line profile is significantly narrower in spectrum C than in the other ones (A and B). This change in near-edge structure as a function of particle charge is assigned as follows: With increasing particle charge the surface potential retains electrons that are emitted after photoabsorption. Near the O 1*s* edge electrons of different kinetic energy are produced, reaching from near zero kinetic energy electrons to fast ones of >500 eV. The slow electrons which are suppressed at higher charge states come from shake-off processes as well as inelastically scattered electrons. These are mostly formed in the bulk. Fast electrons come either from normal and resonant Auger processes as well as direct outer shell photoionization. The latter process is of negligible cross section in the O 1*s* regime and should not vary significantly across the absorption edge. Resonant Auger processes yield the fastest electrons, occurring only upon resonant excitation of preedge resonances. These electrons can still be emitted even at the highest surface potential and contribute to curve C. Previous theoretical work indicates that there are three unoccupied states (T′, T1, and A1) that can be reached upon O 1*s* excitation below 538 eV [20]. Evidently, the resonant Auger spectra of the transitions that contribute to the dominant near-edge feature have distinct properties, so that electrons of different kinetic energy are emitted, where the fastest ones are formed by excitation with photon energies ranging between 533 and 542 eV. Their magnitude is evidently too low so that they are not observed in the charging curve shown in Fig. 2(g). The charging curve C shown in Fig. 3(b) reaches >60 000 charges, corresponding to a surface potential of ~420 V. This value is clearly lower than the photon energy used for charging in the O 1*s* regime. This maximum value is evidently not reached since there are efficient charge loss mechanisms active, as mentioned above. On the other hand, a surface potential of ~420 V cannot retain efficiently KLL-Auger electrons in the O 1*s* continuum. This indicates limitations of the oversimplified model of charge localization on the surface of the spherical particle, used to determine the surface potential. The spectral changes observed in Fig. 3(b) require at least a surface potential of >500 V in order to retain quantitatively all electrons from normal KLL-Auger processes upon O 1*s* ionization. It appears to be rather straightforward that the charges are not uniformly distributed over the particle surface, so that changes in particle radius or defect sites can contribute to charge localization. Recent *ab initio* work indicates, indeed, that twofold coordinated silicon atoms are hole traps in SiO_2 [23].

In conclusion, we have investigated the charging mechanisms of free SiO_2 nanoparticles that are selectively excited in the soft x-ray regime. The number of emitted electrons per absorbed photon changes significantly as a function of photon energy, indicating that both secondary electrons and primary electrons, i.e., photoelectrons and Auger electrons, contribute to particle charging by soft x rays. Furthermore, the number of absorption events with effectively no electron ejection increases with the particle charge. Experiments in the O 1*s* regime indicate that at low charge state the energy dependence of the charging current is similar to that of the photoabsorption of macroscopic SiO_2. At high particle charge only those electrons from resonant Auger processes can contribute to an increase of the charge state.

We thank A. A. Pavlychev for helpful discussions. Financial support by the Bundesministerium für Bildung und Forschung (BMBF) and the Deutsche Forschungsgemeinschaft are gratefully acknowledged.

*Present address: University College Dublin, School of Physics, Belfield, Dublin 4, Ireland.

[1] M. C. Daniel *et al.*, Chem. Rev. **104**, 293 (2004).
[2] K. S. Hamad *et al.*, Phys. Rev. Lett. **83**, 3474 (1999).
[3] H. Döllefeld *et al.*, J. Chem. Phys. **117**, 8953 (2002).
[4] C. Delerue *et al.*, Phys. Rev. Lett. **75**, 2228 (1995).
[5] L.-W. Wang *et al.*, Phys. Rev. Lett. **91**, 056404 (2003).
[6] T. D. Krauss, Phys. Rev. Lett. **83**, 4840 (1999).
[7] P. Kulkarni *et al.*, J. Aerosol Sci. **33**, 1279 (2002).
[8] S. Schlemmer *et al.*, J. Appl. Phys. **90**, 5410 (2001).
[9] D. Gerlich, Hyperfine Interact. **146**, 293 (2003).
[10] S. Arnold *et al.*, Rev. Sci. Instrum. **70**, 1473 (1999).
[11] N. H. Turner *et al.*, Anal. Chem. **70**, 229R (1998).
[12] W. Paul, Rev. Mod. Phys. **62**, 531 (1990).
[13] M. Grimm *et al.*, in *Synchrotron Radiation Instrumentation: Eighth International Conference on Synchrotron Radiation Instrumentation*, edited by T. Warwick, J. Arthur, H. A. Padmore, and J. Stöhr, AIP Conf. Proc. No. 705 (AIP, New York, 2004), p. 1062.
[14] H. W. Biester *et al.*, Phys. Rev. Lett. **59**, 1277 (1987).
[15] R. Santra *et al.*, Phys. Rev. B **64**, 245104 (2001).
[16] N. Saito *et al.*, Int. J. Mass Spectrom. **115**, 157 (1992).
[17] K. Ohya *et al.*, Phys. Rev. B **46**, 3101 (1992).
[18] *CRC Handbook of Chemistry and Physics*, edited by D. R. Lide (CRC Press, Boca Raton, 1993), pp. 12–107, 74th ed.
[19] Z. Y. Wu *et al.*, J. Phys. Condens. Matter **8**, 3323 (1996).
[20] I. Tanaka *et al.*, Phys. Rev. B **52**, 11 733 (1995); A. Marcelli *et al.*, J. Phys. (Paris) **46**, 107 (1985).
[21] S. D. Mo, Appl. Phys. Lett. **78**, 3809 (2001).
[22] M. Taillefumier, Phys. Rev. B **66**, 195107 (2002).
[23] V. A. Gritsenko, Solid State Commun. **121**, 301 (2002).